Precambrian Research 319 (2018) 187–197

Contents lists available at ScienceDirect

Precambrian Research

journal homepage: www.elsevier.com/locate/precamres

Delayed Neoproterozoic oceanic oxygenation: Evidence from Mo isotopes of the Cryogenian Datangpo Formation

Meng Cheng[a], Chao Li[a,*], Xi Chen[b], Lian Zhou[c], Thomas J. Algeo[a,c,d], Hong-Fei Ling[b], Lian-Jun Feng[e], Cheng-Sheng Jin[f,a]

[a] State Key Laboratory of Biogeology and Environmental Geology, China University of Geosciences, Wuhan 430074, China
[b] State Key Laboratory for Mineral Deposits Research, Nanjing University, Nanjing 210046, China
[c] State Key Laboratory of Geological Processes and Mineral Resources, China University of Geosciences, Wuhan 430074, China
[d] Department of Geology, University of Cincinnati, Cincinnati, OH 45221, USA
[e] Institute of Geology and Geophysics, Chinese Academy of Science, Beijing 100029, China
[f] Yunnan Key Laboratory for Palaeobiology, Yunnan University, Kunming 650091, China

ARTICLE INFO

Keywords:
Oxygenation event
Euxinia
Oceanic anoxia
Molybdenum
Early animals
Metazoans

ABSTRACT

The Neoproterozoic oxygenation event (NOE) likely began earlier than 800 Ma, raising oxygen levels in the Earth's atmosphere-ocean system and, thus, setting the stage for the emergence and diversification of animals. However, the redox history of the oceans during the following Cryogenian Period (~720–635 Ma) remains poorly constrained. Here, we present a biogeochemical study based on Mo-isotope (this study) and Fe, C, Mo abundance data (previously reported data) for black shales of the ~660-Ma Datangpo Formation in the Minle section of the Nanhua Basin, South China. Iron speciation data indicate that the study samples were most likely deposited under euxinic conditions. The studied samples yield two clusters of δ^{98}Mo data: +0.98‰ to +1.14‰ [+1.06 ± 0.06 (SD) ‰] and −0.13‰ to +0.68‰ (+0.65 ± 0.31‰), respectively, with the higher values found mostly in the lowermost black shales. The variably lower δ^{98}Mo values probably do not reflect contemporaneous open-ocean seawater composition owing to lower aqueous H_2S concentrations caused by substantial watermass restriction (as evidenced by Mo-TOC covariation patterns), whereas the high δ^{98}Mo values may record contemporaneous Cryogenian seawater values. The seawater δ^{98}Mo values from our study at ~660 Ma are similar to previously reported seawater δ^{98}Mo values at ~750 Ma (+1.11‰) and ~640 Ma (+1.15‰), implying the existence of widespread oceanic anoxia throughout the Cryogenian. Because the subsequent Ediacaran Period shows evidence of greater oceanic oxygenation based on multiple geochemical proxies, our findings suggest that the process of oceanic oxygenation proceeded slowly during the Cryogenian Period. This may have been an important factor in delaying the first appearance of metazoans until the late Cryogenian and their diversification until the Ediacaran.

1. Introduction

The Cryogenian Period (~720–635 Ma) of the Neoproterozoic was an important interval in Earth's history that coincided with the emergence of animals (Erwin et al., 2011), a rapid rise of marine planktonic algae (Brocks et al., 2017; Hoshino et al., 2017), a major tectonic reorganization (Li et al., 2008), intense climate perturbations including the development of 'Snowball Earths' (Hoffman et al., 1998), the onset of the decoupling between organic and inorganic carbon isotopes (Swanson-Hysell et al., 2010), and atmospheric oxygen increases (e.g. Och and Shields-Zhou, 2012; Planavsky et al., 2014). These tectonic, climatic, environmental, and biological events are considered to have been interconnected, one example being the rise in oceanic oxygen levels as a trigger for the emergence of animals (Knoll and Carroll, 1999).

The first metazoans appeared during the Neoproterozoic. The interglacial period between Snowball Earths (~660–640 Ma) may have served as a window for the development of the earliest animals. Maloof et al. (2010) reported possible animal body fossils (sponges) from strata of this age (~659–635 Ma), consistent with biomarker evidence indicating that the simplest animals (i.e., sponges) may have appeared during this period (> 635 Ma) (Love et al., 2009). Despite uncertainty in the age of the first metazoans, it is well established that early animals diversified rapidly following the termination of the Gaskiers Glaciation

* Corresponding author.
E-mail address: chaoli@cug.edu.cn (C. Li).

https://doi.org/10.1016/j.precamres.2017.12.007
Received 6 February 2017; Received in revised form 17 October 2017; Accepted 3 December 2017
Available online 05 December 2017

at ~580 Ma (Xiao and Laflamme, 2009; Xiao et al., 2016).

The oxygenation history of the Neoproterozoic is also subject to uncertainties. Whereas chromium (Cr) isotope data from shales and iron formation support a rise in atmospheric oxygen levels above 0.1% PAL (present atmospheric level) at ~800 Ma (Cole et al., 2016; Planavsky et al., 2014), Cr isotope data from carbonates suggest that this increase in pO_2 occurred earlier, i.e., by the late Mesoproterozoic (~1.1 Ga) (Gilleaudeau et al., 2016). A study of fluid inclusions in evaporites from the Officer Basin of Australia suggests that oxygen levels reached nearly 50% PAL by ca. 815 Ma (Blamey et al., 2016). On the other hand, other datasets suggest that significant oxygenation of the oceans may have been delayed until the Ediacaran or later (Canfield et al., 2007; Dahl et al., 2010; Fike et al., 2006; Kendall et al., 2015; Sahoo et al., 2012; Sperling et al., 2015). Although uranium and iron isotope evidence suggests an episodic/progressive increase of oxygen levels in the ocean shortly after the Sturtian interglacial at ~660–640 Ma (Lau et al., 2017; Zhang et al., 2015), iron speciation and elemental data from the same time interval suggest that strong oceanic anoxia may have persisted at least in some marine basins (e.g. Li et al., 2012; Scott et al., 2008). Thus, geochemical evidence supports a degree of oceanic oxygenation by the end of the Ediacaran (Kendall et al., 2015), but existing uncertainties in the redox history of Cryogenian oceans make evaluation of its relationship to early animal evolution difficult.

Apparent contradictions about the redox state of the Cryogenian oceans may reflect a large degree of spatiotemporal heterogeneity (e.g. Li et al., 2010, 2015) and/or the limited insights provided by local redox proxies (Cheng et al., 2017). Molybdenum isotopes in organic-rich black shales have been shown to be a powerful proxy for assessment of average global-ocean redox conditions in the past (Arnold et al., 2004; Dahl et al., 2010). However, one of the difficulties in generating long-term paleo-ocean oxygenation records based on this proxy is the uneven distribution of black shales in space and time. For example, black shales are relatively rare during the Late Cryogenian interval of Snowball Earth development. The presence of ~660-Ma black shales in the Datangpo Formation of the Nanhua Basin of South China thus provides an opportunity to track the evolution of Late Cryogenian global-ocean redox conditions. The only existing Mo-isotope study from this interval investigated strata dating to ~640 Ma, i.e., the late stage of the post-Sturtian interglacial (Kendall et al., 2015). In this study, we analyze black shales of the lowermost Datangpo Formation, dating to ~660 Ma, in order to explore possible changes in oceanic redox conditions during the early post-Sturtian interglacial. We assess our results in the context of the oxygenation history of the atmosphere and oceans throughout the Cryogenian Period and draw inferences concerning its relationship to the evolution of the earliest animals.

2. Geological setting

During the Neoproterozoic, South China consisted of two separate terranes, the Yangtze Block and the Cathaysia Block (Fig. 1A). Beginning at ~850 Ma, a series of large mantle plume events led to the breakup of the supercontinent Rodinia (Li et al., 2003). As a result, the Nanhua Basin developed as a rift basin along the southern margin of the Yangtze Block and progressively evolved into a passive continental margin during the Ediacaran (Jiang et al., 2003; Wang and Li, 2003). Paleogeographic reconstructions show that water depths increased southeastward across the Yangtze Block during the interglacial Cryogenian, and a semi-restricted basin was likely formed (Fig. 1B; Wang and Li, 2003). The Nanhua Basin accumulated a thick sedimentary succession from the mid-Neoproterozoic to the Ordovician. Two glacial diamictite intervals (the lower Gucheng/Tiesiao/Changan Formation and the upper Nantuo Formation) corresponding to the global Sturtian and Marinoan Glaciations serve as important stratigraphic markers within this succession. The Cryogenian consists mainly of glacial tillite and interglacial shales, whereas the Ediacaran consists of mixed carbonate-siliciclastic units (Jiang et al., 2011).

The Datangpo Formation occurs between the Sturtian and Marinoan glacial diamictites and associated glaciogenic strata. This formation contains a characteristic sequence of lithologies, including (from the base of the unit upwards) manganese-bearing carbonate, black shale, and siltstone, reflecting a gradual long-term shoaling (Wang and Li, 2003). The thickness of the Datangpo Formation varies from < 130 m in shelf areas to > 500 m in the basin center (Wang and Li, 2003). U-Pb ages from near the base and top of this formation indicate that deposition occurred between 663 ± 4 Ma (Zhou et al., 2004) and 654.5 ± 3.8 Ma (Zhang et al., 2008).

The Minle section is located in Minle Town, Huayuan County, in northwestern Hunan Province. At Minle, the Datangpo Formation is ~220 m thick, representing an average sedimentation rate of ~24 m Myr^{-1}. Here, the Datangpo Formation consists of (1) a basal carbonate member, including a lower dolomite bed (< 1 m thick) and an upper Mn-carbonate bed (~2 m thick, mainly rhodochrosite) (not to scale in Fig. 1C), (2) a lower black shale member (~30 m thick), and (3) an upper grey shale member (~180 m thick) (Fig. 1C). In the gray shale member and upper portion of the black shale member (i.e., > 20 m in Fig. 1C), the strata mainly accumulated under oxic/suboxic (anoxic porewater but oxic water column) conditions, as shown by Fe speciation analysis (Feng et al., 2010; Li et al., 2012). The samples show no enrichment in Mo, and thus are not suitable for Mo isotope analysis. For this reason, we focused our investigation on the lower portion of the black shale member of the Datangpo Formation (0–20 m in Fig. 1C), which Fe speciation data indicate to have been deposited under euxinic conditions (Feng et al., 2010; Li et al., 2012). At the average sedimentation rate cited above, the 20-m-thick study interval represents < 1 Myr of sediment accumulation around 660 Ma.

3. Methods

Fifteen samples were selected and analyzed for Mo-isotope compositions (δ^{98}Mo) in this study. The study section is the same as that analyzed for S isotopes and Fe speciation by Feng et al. (2010) and Li et al. (2012). However, all samples were collected from the same outcrop by the same research group using the same field logging system and, thus, can be integrated into a single dataset without concern about stratigraphic mismatches. Sample powders (~200 mesh) were ashed at 600 °C for ~8 h to remove organic matter. For Mo isotope analysis, 10–100 mg (depending on the Mo content) of oxidized powder were weighed into a Teflon bomb. After addition of a ^{97}Mo-^{100}Mo double spike, each sample was digested first with HF + HNO_3 at 190 °C for 48 h and then with HCl at 120 °C for 10 h. Afterward, the solution was dried, re-dissolved, and processed using ion-exchange chromatography to separate Mo from the sample matrix using a two-stage column procedure with chelating resins described in Cheng et al. (2016) and Chen et al. (2015). The resins GPM-1M and AG50-X8 (Bio-Rad) allowed recovery of > 95% of total Mo. Mo isotope compositions were determined by a Thermal Scientific Neptune multicollector-inductively coupled plasma-mass spectrometry. Samples from Feng et al. (2010) were analyzed in the SKL-GPMR (State Key Laboratory of Geological Processes and Mineral Resources) of the China University of Geosciences (Wuhan) and samples from Li et al. (2012) were analyzed in the SKL-MDR (State Key Laboratory for Mineral Deposits Research) of Nanjing University. The data are reported as parts per thousand (‰) variation of δ^{98}Mo relative to the Johnson Matthey ICP Mo standard solution (lot 602332B) and NIST SRM 3134, which were used in SKL-GPMR and SKL-MDR, respectively, where δ^{98}Mo is defined as $(^{98/95}Mo_{sample}/^{98/95}Mo_{standard} - 1) \times 1000$. The long-term external reproducibility of the isotope ratio measurements on the mass spectrometer is less than 0.09‰ (± 2 SD). Data from the SKL-GPMR were recalculated relative to NIST SRM 3134 = 0.25‰ as described by Goldberg et al. (2013). Then, a correction for detrital Mo was made

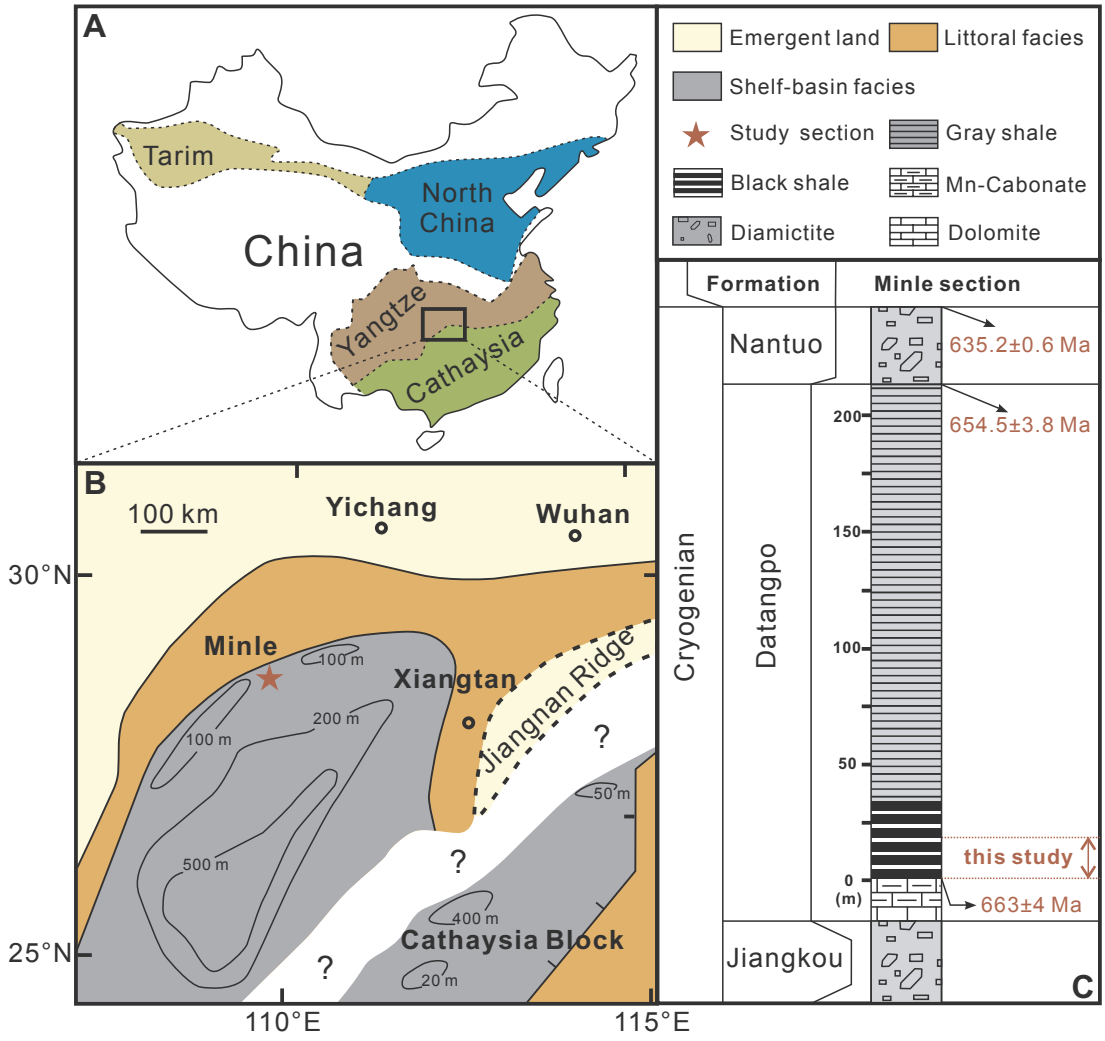

Fig. 1. Geological setting of the Nanhua Basin in South China. (A) Tectonic background of Nanhua Basin. (B) Paleogeographic and paleobathymetric map of the Cryogenian Nanhua Basin (modified from Wang and Li, 2003). (C) Stratigraphic column of the Datangpo Formation at Minle section (modified from Feng et al., 2010). The redioactive ages of 635.2 ± 0.6 Ma, 654.5 ± 3.8 Ma and 663 ± 4 Ma are from Condon et al. (2005), Zhang et al. (2008) and Zhou et al. (2004), respectively. (For interpretation of the references to colour in this figure legend, the reader is referred to the web version of this article.)

following Eqs. (1) and (2) using the following values: Al_{det} = 8.04%, Mo_{det} = 1.5 ppm, and $\delta^{98}Mo_{det}$ = +0.40‰ (Dahl et al., 2011; McLennan, 2001). All of the δ^{98}Mo data in the Discussion section of this study refer to the authigenic component, i.e. $\delta^{98}Mo_{auth}$.

$$f_{det} = \left(\frac{Mo_{det}}{Al_{det}}\right) \times \frac{Al_{sample}}{Mo_{sample}} \quad (1)$$

$$\delta^{98}Mo_{auth} = (\delta^{98}Mo_{sample} - f_{det} \times \delta^{98}Mo_{det})/(1-f_{det}) \quad (2)$$

We note that Cole et al. (2017) challenged use of a single average crustal value in correcting for the detrital fraction. However, when the detrital Mo fraction is small, as in the present study (< 15%, average 11%), uncertainties in $\delta^{98}Mo_{auth}$ related to crustal compositional values are negligible (< 0.05‰). Even if the lowest crustal value of 0‰ was used for the correction, the $\delta^{98}Mo_{auth}$ increases only by ~0.1‰. Consequently, our correction method results in only limited uncertainty in absolute $\delta^{98}Mo_{auth}$ estimates and does not affect the secular trends in $\delta^{98}Mo_{auth}$ reported in this study.

4. Results

The Mo-isotope data collected in this study and accompanying geochemical data published previously for the Datangpo Formation in the Minle section are given in Table 1 and summarized in Fig. 2. δ^{98}Mo ranges from −0.13‰ to +1.14‰, but the δ^{98}Mo profile shows two discrete intervals: (1) the lowermost 6 m is characterized by higher and relatively uniform δ^{98}Mo (+0.98‰ to +1.14‰, average +1.06 ± 0.06 (1σ) ‰), and (2) the interval at 6–20 m is characterized by lower and more variable δ^{98}Mo (−0.13‰ to +0.68‰, average +0.65 ± 0.31‰).

5. Discussion

5.1. Bottom-water redox conditions of the Nanhua Basin

The Fe speciation data for the Minle section reported by Feng et al. (2010) and Li et al. (2012) are used here as an independent geochemical proxy to evaluate bottom-water redox conditions. Chemically active iron can be redistributed through redox cycling from oxic shelves to deeper anoxic basins (Lyons and Severmann, 2006). Moreover, if euxinia develops in the deepwater environment, reactive iron can react with aqueous H_2S, forming pyrite that accumulates in the sediment. Thus, anoxic marine sediments generally have high concentrations of reactive Fe (Fe_{HR}), which includes pyrite (Fe_{py}) and other Fe phases [e.g. ferric oxides (Fe_{ox}), magnetite (Fe_{mag}), and carbonate minerals (Fe_{carb})] that can form pyrite through reaction with H_2S during early

Table 1
Geochemical data of the Datangpo black shales at Minle.[a]

Sample	Lithology	Depth m	Fe_T wt.%	Fe_{py} wt.%	Fe_{HR}/Fe_T	Fe_{py}/Fe_{HR}	TOC wt.%	Mo ppm	Al[b] wt.%	Mo/TOC ppm/%	$\delta^{98}Mo$[c] ‰	$\delta^{98}Mo_{auth}$[d] ‰
ML68	Black shale	18.8	4.48	1.92	0.64	0.67	3.64	6.0	8.14	1.6		
ML-11	Black shale	17	0.60	0.00	0.10	0.30	4.70	10.4	7.00	2.2		
ML70	Black shale	16.8	2.32	1.07	0.67	0.69	4.77	18.0	8.01	3.8	0.50	0.50
ML-10	Black shale	16	0.30	0.20	0.70	0.90	3.90	3.8	6.80	1.0		
ML-09	Black shale	15	0.40	0.20	0.40	1.00	3.6	5.0	7.30 av	1.4	0.05	-0.06
ML72	Black shale	14.8	3.68	0.69	0.36	0.52	3.77	12.0	8.47	3.2	0.43	0.43
ML-08	Black shale	14	0.30	0.20	0.50	1.00	3.10	8.6	9.00	2.8	0.07	0.00
ML74	Black shale	12.8	4.39	1.94	0.68	0.65	2.77	20.0	9.10	7.2	0.52	0.53
ML-07	Black shale	12	0.40	0.20	0.40	0.90	2.10	10.2	10.10	4.9	-0.04	-0.13
ML-06	Black shale	11	0.40	0.20	0.40	1.00	1.90	3.6	10.90	1.9		
ML-05	Black shale	10	1.90	0.20	0.10	0.80	2.00	14.0	7.10	7.0	0.34	0.34
ML77	Black shale	9.8	5.24	2.11	0.66	0.61	2.56	22.0	8.97	8.6	0.94	1.02
ML-04	Black shale	9	2.40	2.30	1.00	0.90	2.40	15.0	4.20	6.3	0.66	0.68
ML-03	Black shale	8	1.70	2.00	1.00	0.90	1.60	7.0	5.70	4.4	0.61	0.66
ML-02	Black shale	7	2.60	1.90	0.90	0.80	1.70	9.0	7.30 av	5.3	0.60	0.65
ML-01	Black shale	6	4.40	1.92	1.00	0.90	1.90	39.0	7.60	20.5	1.07	1.10
ML79	Black shale	6.8	4.16	3.70	0.66	0.70	2.61	31.0	7.63	11.9		
ML80	Black shale	4.8	0.38	0.01	0.26	0.09	1.87	7.0	10.95	3.7		
ML81	Black shale	2.3	1.83	0.69	0.60	0.63	1.67	29.0	7.94	17.4	0.94	0.98
ML82	Black shale	0.4	2.56	1.64	0.80	0.80	1.84	37.0	11.04	20.1	1.01	1.07
ML83	Black shale	0	0.6	0.38	0.88	0.72	1.92	29.0	8.01	15.1	1.08	1.14

[a] Mo-isotope data are from this study while rest data are from Feng et al. (2010) (ML68 to ML83) and Li et al. (2012) (ML-01 to ML-11).
[b] The superscript "av" refer to the average Al concentration of all samples since no data were reported in the original study.
[c] Mo isotope data of ML68 to ML83 are reported relative to JMC and samples of ML-01 to ML-11 are reported relative to NIST SRM 3134 = 0.25‰.
[d] Mo isotope data are reported relative to NIST SRM 3134 = 0.25‰ and corrected for the detrital contribution.

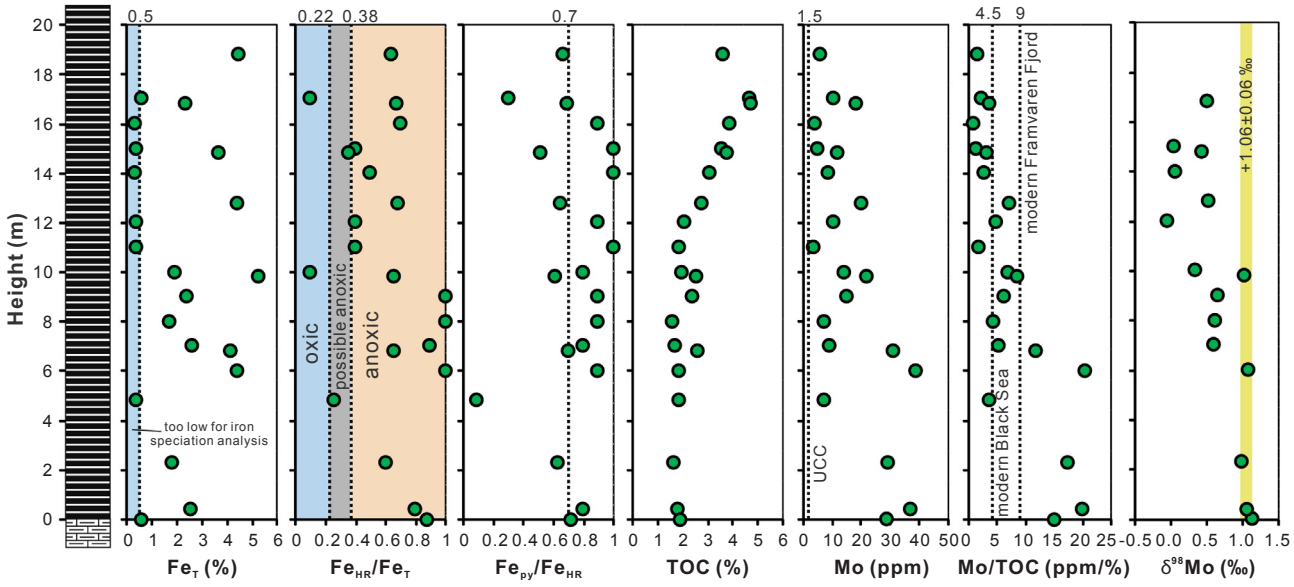

Fig. 2. Integrated chemostratigraphy of the Datangpo Formation at Minle. The black dashed lines represent the threshold values and the yellow band represents the average of the higher Mo isotopes (+1.06 ± 0.06‰). The δ^{98}Mo data are original to this study; the remaining data were compiled from Feng et al. (2010) and Li et al. (2012). UCC = upper continental crust.

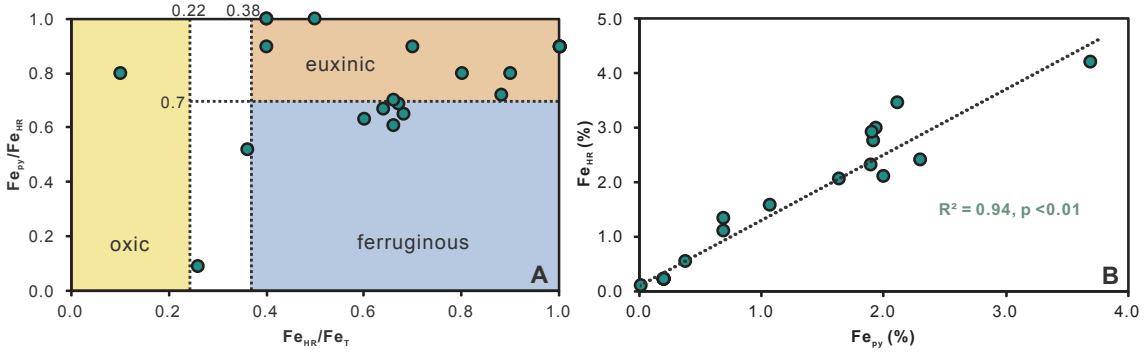

Fig. 3. Crossplots of Fe_{py}/Fe_{HR} versus Fe_{HR}/Fe_T (A), and Fe_{HR} versus Fe_{py} (B) for samples from the Datangpo black shales at Minle.

burial. Generally, the ratio of Fe_{HR} to total Fe (Fe_T) is < 0.22 in oxic facies but > 0.38 in anoxic facies (Poulton and Canfield, 2011). Given Fe_{HR}/Fe_T values that are indicative of anoxia, Fe_{py}/Fe_{HR} > 0.7 suggests euxinic conditions (i.e., aqueous H_2S) and Fe_{py}/Fe_{HR} < 0.7 suggests ferruginous conditions (i.e., aqueous Fe^{2+}) (Poulton and Canfield, 2011; Raiswell and Canfield, 1998). However, these thresholds are not absolute, and redox interpretations can be uncertain when samples plot close to the boundaries; in this case, crossplots between different Fe species may help to clarify redox conditions (Li et al., 2012).

The Datangpo black shale samples show variable Fe_{HR}/Fe_T and Fe_{py}/Fe_{HR} ratios (Fig. 2). Iron concentrations vary significantly, especially in the upper part of the section (Fig. 2). Since low Fe_T contributes to low analytical precision in Fe-speciation analysis, only samples with Fe_T > 0.5% are considered here. Most samples show Fe_{HR}/Fe_T ratios > 0.38, indicating an anoxic depositional environment (Fig. 3A). The Fe_{py}/Fe_{HR} ratios of these samples vary from 0.61 to 0.90, straddling the boundary between euxinic and ferruginous conditions (Fig. 3A). Because the study samples were collected from outcrop, it is possible that some of the Fe_{py} was converted to Fe_{ox}, making the measured Fe_{py}/Fe_{HR} ratios minimum values. However, Fe_{ox} comprises only a minor proportion of Fe_{HR} (< 10%), and no negative correlation is observed between Fe_{py} and Fe_{ox}, which argue against significant weathering influences on our samples (Feng et al., 2010; Li et al., 2012). On the other hand, a strong linear relation is observed between Fe_{py} and Fe_{HR} (R^2 = 0.94, p < 0.01) (Fig. 3B), suggesting that the amount of pyrite iron was regulated by the availability of Fe_{HR} rather than H_2S (Li et al., 2012). Although this does not negate the possibility of transiently ferruginous or fluctuating redox conditions (e.g. Cheng et al., 2017), we infer that the Datangpo black shales are likely to have accumulated under dominantly euxinic conditions.

5.2. Hydrographic conditions of the Nanhua Basin and Cryogenian oceanic Mo reservoir

The behavior of Mo in seawater is mainly a function of ambient redox conditions. In oxic waters, Mo is present as the soluble, conservative molybdate anion (MoO_4^{2-}), generally leading to little authigenic enrichment of the sediment above continental crustal background concentrations (1–2 ppm), although slowly accumulating Fe-Mn nodules and crusts are sometimes enriched to hundreds of parts per million (Algeo and Maynard, 2004). In contrast, the Mo removal rate is 100- to 1000-fold greater in euxinic waters than in oxic waters, leading to large authigenic enrichments that can exceed 100 ppm (Dahl et al., 2013b; Scott and Lyons, 2012; Scott et al., 2008). In weakly oxygenated waters with sulfidic conditions developed in the porewaters, Mo is mildly enriched in the underlying sediments. In the modern oceans, Mo concentrations in such settings are < 25 ppm (Scott and Lyons, 2012), but values in comparable settings may have been much lower in more poorly oxygenated Proterozoic oceans. Ferruginous watermasses may not accumulate large amounts of authigenic Mo because most adsorbed Mo will be released back to the water column during early diagenetic processing (Cheng et al., 2016; Morford et al., 2009). Despite having been deposited under euxinic conditions (see Section 5.1), the Datangpo black shales show rather low Mo concentrations (6–36 ppm, average 21 ppm), which are significantly lower than those of modern permanently euxinic environments (Dahl et al., 2013b; Scott and Lyons, 2012).

In addition to local redox variation, seawater Mo availability also influences authigenic Mo enrichment (Algeo and Lyons, 2006). Since our samples were mostly deposited under euxinic conditions (see Section 5.1), the low Mo abundance of the Datangpo black shales was most likely a consequence of limited aqueous Mo availability during their deposition. The degree of basinal restriction and the size of the global oceanic Mo reservoir are the two main factors controlling seawater Mo availability in a marginal basin (Algeo and Lyons, 2006; Scott et al., 2008).

Generally, a positive linear relationship is observed between Mo and total organic carbon (TOC) concentrations in sediments, indicating the importance of organic carbon for authigenic Mo uptake (Algeo and Lyons, 2006). This relationship may result from adsorption of thiomolybdates [$MoO_{4-x}S_x^{2-}$(x= 1–4)], which form from MoO_4^{2-} under the influence of H_2S and are particle-reactive to organic matter (Algeo and Lyons, 2006; Dahl et al., 2016). However, other pathways of authigenic Mo enrichment, e.g., formation of Fe-Mo-S nano-minerals (Helz et al., 2011), are also possible. These processes are often associated with reduction of Mo from +6 to +4 (Dahl et al., 2013a). Thus, the linear relationship between Mo and TOC may reflect the roles of organic matter as a substrate during trace-metal adsorption and/or as an electron donor during reduction. By normalizing Mo concentrations to TOC, the Mo/TOC ratio removes the effect of variable organic carbon concentrations in the sediment and, thus, serves as a proxy for Mo availability in the seawater source reservoir (Algeo and Lyons, 2006).

In modern restricted marine basins, a linear relationship between seawater Mo concentrations and sediment Mo/TOC ratios is observed, supporting Mo/TOC as a proxy for seawater Mo availability in modern and ancient oceans (Algeo and Lyons, 2006). Importantly, the Mo/TOC ratio can also provide information about the secular dynamics of semi-restricted basins; for example, after a deepwater renewal event by open-ocean waters, Mo concentrations may spike and then decline slowly as aqueous Mo is drawn down, even as TOC holds steady or increases owing to an intensification of reducing conditions between deepwater renewal events (Fig. 4A) (Algeo and Lyons, 2006). Although their Mo enrichments are much lower relative to modern euxinic sediments (see above), this pattern of secular covariation of Mo and TOC is observed in the Datangpo black shales (Fig. 4B), suggesting that (1) semi-restricted hydrographic conditions occurred in the Nanhua Basin during the

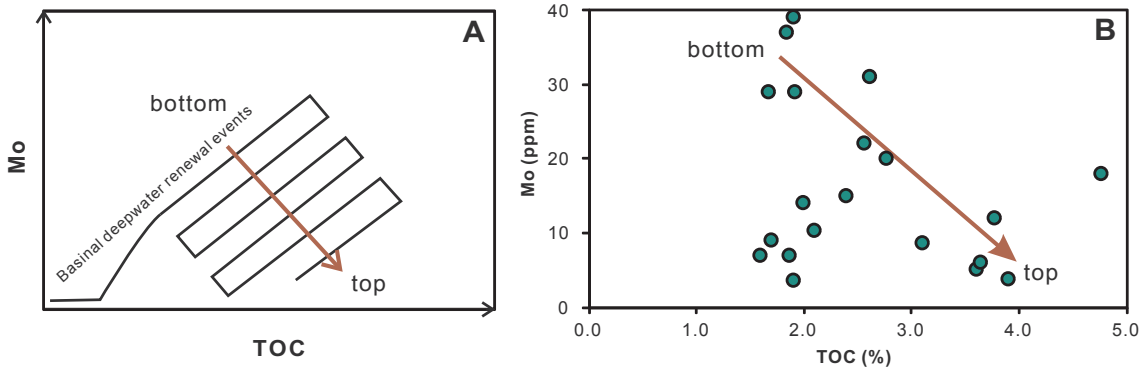

Fig. 4. Crossplots of sedimentary Mo versus total organic carbon content (TOC) for theoretical prediction of silled euxinic basins (A) and for samples from the Datangpo black shales (B). The model is modified from Algeo and Lyons (2006). The red arrowed lines indicate the direction from the bottom to top of the silled euxinic basin sediments in (A) and of study section in (B). See text for detailed explanation.

interglacial interval, consistent with paleogeographic reconstructions (Wang et al., 2003; Fig. 1B) and (2) aqueous Mo availability was limited through Mo uptake by the sediments at this time.

In addition to basinal restriction, the size of the Mo reservoir in the global ocean at a given time in the past can influence seawater Mo availability. The uniformly low aqueous Mo availability in the interglacial Nanhua Basin (Fig. 4B; see above) suggests that the Cryogenian oceanic Mo reservoir was small. Given that individual basins are subject to both local and global effects, recognition of the global signal requires compilation of Mo/TOC data from multiple coeval basins. The compilation of Scott et al. (2008) suggests that the early Neoproterozoic was characterized by low seawater Mo concentrations compared to the Phanerozoic, although the available data for this interval are still rather limited.

5.3. Controlling factors on Mo isotopic composition of Datangpo black shales

5.3.1. Hydrological restriction of the Nanhua Basin

In the Cryogenian, the Nanhua Basin was a silled basin that gradually evolved into a semi-closed basin during deposition of the Datangpo Formation (see Section 5.2). This hydrological change may have affected seawater δ^{98}Mo in the basin and, in turn, sediment δ^{98}Mo. Seawater δ^{98}Mo in a semi-closed marginal basin is determined by the relative contributions from riverine Mo versus global-ocean Mo. In the modern Black Sea, aqueous Mo is mainly seawater-sourced, despite only a limited connection with the Mediterranean through the Bosporus Strait (Neubert et al., 2008). In such systems, open-ocean-derived Mo predominates because of the much higher Mo concentration in seawater relative to river water (105 nM vs. an average of 6 nM for the modern) (Archer and Vance, 2008; Collier, 1985).

The Cryogenian oceanic Mo reservoir was much smaller than today's (see Section 5.2 and Scott et al., 2008), so riverine Mo inputs may have been relatively more important to seawater δ^{98}Mo in restricted marginal-marine basins. Modern riverine Mo shows a broad range of δ^{98}Mo values with an average of +0.7‰ (Archer and Vance, 2008), which is much lower than the modern seawater δ^{98}Mo of +2.3‰. Therefore, input of riverine water will lower seawater δ^{98}Mo in a restricted marginal basin. The average crustal δ^{98}Mo signature (0 to +0.4‰) likely has not fluctuated much during Earth's history because magmatic processes result in very limited Mo isotopic fractionations (Voegelin et al., 2014; Yang et al., 2017). In the Cryogenian, the δ^{98}Mo of the riverine source to the ocean was likely intermediate between crustal and modern average riverine δ^{98}Mo values (i.e., 0 to +0.7‰) although the local rivers draining into the Nanhua Basin may have had δ^{98}Mo values different from those of modern rivers. Therefore, if evolution of the Nanhua Basin into a more restricted basin during deposition of the Datangpo Formation led to relatively greater Mo inputs from riverine sources, then watermass δ^{98}Mo and, in turn, sedimentary δ^{98}Mo would have decreased. Indeed such a δ^{98}Mo trend is observed in the Datangpo black shales (Fig. 2), consistent with increasing riverine control upsection within the study units.

For seawater δ^{98}Mo to be nearly identical to that of its riverine source requires an extremely small marine Mo reservoir, which would lead to negligible authigenic Mo accumulation in the sediments (Wille et al., 2008). Although Mo concentrations in Datangpo Formation samples with lighter δ^{98}Mo values are indeed lower than samples with uniformly high δ^{98}Mo (average 11.9 ppm vs. 31.2 ppm, $p < 0.01$), they are still much higher than typical crustal values (~1–2 ppm). Moreover, we note that any mixing of Mo from multiple sources is unlikely to result in basinal δ^{98}Mo values that are outside the range of the end-member components of the mixed system. In the Minle section, two samples show δ^{98}Mo values as low as −0.06‰ and −0.13‰, which is probably lower than the riverine source and, thus, provides evidence for additional controls on the Mo-isotopic composition of the lower Datangpo black shales (see Section 5.3.2).

5.3.2. Local redox variations and variable $[H_2S]_{aq}$ concentrations

Sedimentary δ^{98}Mo is closely related to local watermass redox conditions. In oxic waters, Mo is readily scavenged by adsorption to Fe-Mn oxides, with a stable fractionation between Mn-adsorbed Mo and seawater ($\delta^{98}Mo_{seawater} - \delta^{98}Mo_{Mn\text{-}absorbed} = 3‰$) and variable fractionations between Fe-adsorbed Mo and seawater ($\delta^{98}Mo_{seawater} - \delta^{98}Mo_{Mn\text{-}absorbed} = 0.83–2.19‰$) depending on the mineral types (Barling and Anbar, 2004; Goldberg et al., 2009). As argued in Section 5.1, iron speciation data for the Datangpo Formation indicate a euxinia water column in our study area. Therefore, the influence of Fe-Mn adsorption was less significant.

In euxinic facies, Mo isotopic fractionation is closely related to aqueous H_2S concentrations ($[H_2S]_{aq}$). When $[H_2S]_{aq}$ exceeds the threshold value of 11 ± 3 μM, most aqueous MoO_4^{2-} is transformed to MoS_4^{2-} and quantitatively removed to the sediment (Helz et al., 1996). Under these conditions, Mo isotopic fractionation will be zero and the sediment will acquire a Mo-isotope signature equal or close to $\delta^{98}Mo_{sw}$ ($\delta^{98}Mo_{sw} - \delta^{98}Mo \leq 0.5‰$) (Barling et al., 2001; Nägler et al., 2011; Neubert et al., 2008; Siebert et al., 2006). When $[H_2S]_{aq}$ is < 11 ± 3 μM, Mo uptake by the sediment is accompanied by a fractionation of up to −3‰, and a positive correlation is observed between δ^{98}Mo and $[H_2S]_{aq}$ (Neubert et al., 2008; Poulson et al., 2009).

Local $[H_2S]_{aq}$ concentrations are controlled by multiple factors. H_2S is derived from the reduction of sulfate during microbial decay of organic matter, and it can be re-oxidized to sulfate, form pyrite through reaction with reactive iron, or decompose into HS^-, S^{2-} and $[H_2S]_{aq}$, with the latter closely related to the pH and temperature (Canfield, 1999). For these reasons, local $[H_2S]_{aq}$ concentrations can change even at short timescales (months to years) (Arnold et al., 2012), leading to variable sedimentary δ^{98}Mo, unless local $[H_2S]_{aq}$ remains persistently > 11 μM. The Fe speciation proxy indicates a euxinic water column for the Minle section, but this proxy is insensitive to transient redox variations (Cheng et al., 2017; Tessin et al., 2016) or changes in $[H_2S]_{aq}$. In fact, ferruginous water conditions may have existed at least part of the time because Fe_{py}/Fe_{HR} was close to 0.7. The cluster of samples with uniform, higher δ^{98}Mo values (+1.06 ± 0.06‰) formed under either stable or variable $[H_2S]_{aq}$ above the 11 μM threshold, which is consistent with little to no fractionation between the sediments and contemporaneous seawater. Conversely, the cluster of samples with more variable and lower δ^{98}Mo values (−0.13‰ to +0.68‰) may reflect variation at $[H_2S]_{aq}$ lower than 11 μM during their deposition.

Positive linear correlations between δ^{98}Mo and Mo/TOC ($R^2 = 0.63$, $p < 0.01$; Fig. 5A) and between δ^{98}Mo and Mo concentrations ($R^2 = 0.64$, $p < 0.01$; Fig. 5B) are observed. These correlations possibly indicate that the Mo isotope ratios, Mo availability, and $[H_2S]_{aq}$ in the Nanhua Basin covaried strongly. The lower Datangpo black shales accumulated when the Nanhua Basin was relatively well-connected to the open ocean, and their highest δ^{98}Mo value (+1.1‰) may therefore record that of contemporaneous global seawater at ~660 Ma (see Section 5.2). The Datangpo samples with the highest δ^{98}Mo values show relatively high Mo concentrations (mean 31.2 ppm) and high Mo/TOC values (mean 15 ppm/wt.%). These values are higher than for sediments in the modern semi-restricted Black Sea (~4.5 ppm/wt.%) and Framvaren Fjord (~9 ppm/wt%) (Algeo and Lyons, 2006), suggesting higher Mo concentrations in Nanhua Basin seawater. In contrast, the upper Datangpo black shales accumulated when the Nanhua Basin was more restricted, which may have resulted in a significant reduction in sulfate relative to the contemporaneous open ocean (see Section 5.2) and, thus, to lower $[H_2S]_{aq}$, lower Mo concentrations, and lower δ^{98}Mo in the sediment.

5.4. Mo isotopic composition of Cryogenian seawater and oxidation state of the global Cryogenian ocean at ~660 Ma

The δ^{98}Mo of modern seawater is uniform because the residence time of Mo in the ocean (~440 kyr) is much longer than the mixing

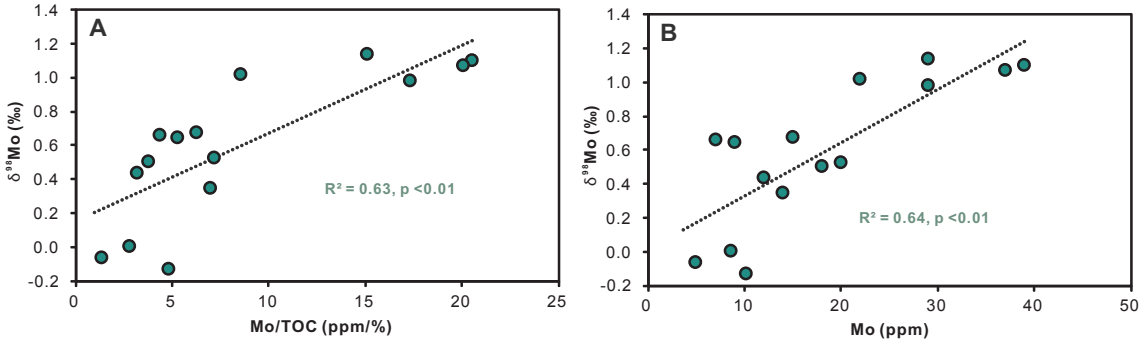

Fig. 5. Crossplots of δ^{98}Mo versus Mo/TOC (A) and δ^{98}Mo versus Mo concentration (B) for samples from the Datangpo black shales at Minle. TOC = Total Organic Carbon content.

time of seawater (~1–2 kyr) (Miller et al., 2011). In the Cryogenian ocean, the Mo reservoir was much smaller (see Section 5.2) and had a correspondingly shorter residence time, resulting in spatially heterogeneous δ^{98}Mo. The low Mo concentrations of global seawater at that time may have had biological consequences. For example, Mo is an important cofactor in nitrogen fixation, and if seawater Mo concentrations fall below ~5% of the level in the modern ocean, organic productivity is likely to decline (Anbar and Knoll, 2002; Zerkle et al., 2006). This process would generate a negative feedback on the abundance of Mo in seawater, because lowered productivity would lead to less intensely reducing conditions, and therefore a less vigorous sink for Mo removal to the sediment (Anbar and Knoll, 2002; Zerkle et al., 2006). This negative feedback would be expected to sustain seawater Mo concentrations at ≥5% of their modern value through time. If the Mo budget of the modern ocean is typical of the past (Reinhard et al., 2013), then 5% of the modern seawater Mo concentration is equivalent to a residence time of ~22 kyr (Miller et al., 2011). This value is still much longer than the seawater mixing time of ~1–2 kyr, so we infer that Mo in the ocean of the study interval was probably well mixed.

Mn-carbonate ores at the base of the Datangpo Formation yielded a δ^{98}Mo of +1.6‰ (Chen et al., 2015), which is higher than the inferred seawater δ^{98}Mo (+1.1‰) from the Minle section. Fe speciation data for these Mn-carbonates indicated an anoxic but ferruginous depositional environment (Fe_{HR}/Fe_T = 0.24–0.71, average 0.45; Fe_{py}/Fe_{HR} = 0.19–0.62, average 0.35), which may have led to significant Mo-isotopic fractionations between the sediments and contemporaneous seawater. A two-stage process of Mo uptake has been proposed for their formation: initial formation as Mn-oxides in the water column, followed by decomposition and reprecipitation as Mn-carbonates in sediment porewaters (Zhang et al., 2013). During this process, Mo adsorbed by Mn-oxides in the water column would have been released into the porewater, which may have superimposed complex fractionation effects linked to an oxic water column with effects from anoxic pore waters, yielding a Mo-isotopic signal in the closed system (Morford et al., 2009), with values that could be higher than those of contemporaneous seawater (Reitz et al., 2007).

The oxygenation state of the global ocean at a given time in the past can be estimated from contemporaneous seawater Mo isotopes using an isotopic mass-balance model (Arnold et al., 2004; Chen et al., 2015; Dahl et al., 2010). In today's oceans, Mo removal to oxic-suboxic facies and euxinic facies represents 35–50% and 5–15% of the total Mo sink flux, respectively (Dahl et al., 2010; Scott et al., 2008). Adsorption of Mo by Mn-oxides in oxic facies results in a fractionation of –3‰ relative to seawater Mo, whereas adsorption of Mo by Fe-oxides/oxyhydroxides in suboxic facies results in a fractionation of −0.8‰ to −2.2‰ relative to seawater Mo (Barling and Anbar, 2004; Goldberg et al., 2009; Poulson et al., 2009). As a consequence, the composition of modern seawater (+2.3‰) is substantially higher than riverine δ^{98}Mo (average +0.7‰) (Siebert et al., 2003). When the global ocean becomes more widely oxic, the removal of isotopically light Mo is enhanced, driving seawater δ^{98}Mo ($\delta^{98}Mo_{SW}$) to higher values.

An isotopic mass-balance model has been used in a number of studies to reconstruct the average global-ocean oxygenation state based on $\delta^{98}Mo_{sw}$ (Arnold et al., 2004; Chen et al., 2015; Dahl et al., 2010), and, for this reason, we refer the reader to Dahl et al. (2011) for a detailed description of the model. For an ocean in steady-state:

$$F_R\delta_R + F_H\delta_H = F_O\delta_O + F_{SAD}\delta_{SAD} + F_E\delta_E \quad (3)$$

where F = flux, δ = δ^{98}Mo, R = rivers, H = low-temperature hydrothermal fluids, O = oxic waters, SAD = sulfidic at depth and weakly euxinic waters ($[H_2S]_{aq}$ < 11 μM), and E = strongly euxinic waters ($[H_2S]_{aq}$ > 11 μM).

The left side of Eq. (3) represents Mo inputs from rivers and low-temperature hydrothermal fluids, which are assumed to have invariant δ^{98}Mo values of +0.4‰ and +0.8‰, respectively (Dahl et al., 2011; McManus et al., 2002). The right side of Eq. (1) represents Mo removals from the ocean in oxic settings (O), sulfide accumulating at depth inside the sediments plus weakly euxinic settings (SAD), and strong euxinic environments (E), which yield Mo isotopic fractionations of ca. −3‰, −0.7‰, and 0‰, respectively, relative to seawater Mo (Barling and Anbar, 2004; Chen et al., 2015; Poulson et al., 2006). If oxic sinks dominate the total sink flux, then $\delta^{98}Mo_{SW}$ will shift toward modern seawater isotope value (+2.3‰). Conversely, if euxinic sinks dominate the total sink flux, then $\delta^{98}Mo_{SW}$ will shift toward that of the riverine sources (+0.7‰). Thus, from the perspective of euxinic facies, higher $\delta^{98}Mo_{SW}$ values signals more oxic conditions, and lower $\delta^{98}Mo_{SW}$ values indicate more reducing conditions in the global ocean.

Previous studies have reported a much lower than modern $\delta^{98}Mo_{SW}$ (+1.0‰) for the mid-Proterozoic, implying greatly expanded areas of reducing sedimentation in oceans of that age (Arnold et al., 2004; Kendall et al., 2009). Similarly, a $\delta^{98}Mo_{SW}$ of +1.1‰ for the Datangpo black shales suggests that the oxygenation state of the global ocean was much lower at ~660 Ma than today. Although large uncertainties exist in the modeling calculation described above, a seawater Mo isotope composition of +1.1‰ implies an oceanic redox state in which Mo removal to strongly euxinic facies was roughly ~30–70% and to oxic facies was less than 15%, contrasting with modern values of ~5–15% for strongly euxinic sinks and ~35–50% for oxic sinks (Chen et al., 2015; Dahl et al., 2011, 2010; Kendall et al., 2017). This conclusion is consistent with a stratified ocean-redox model for the Cryogenian in which oxic waters developed only in the ocean-surface layer, euxinic waters existed at mid-depths (thermocline region), and ferruginous waters dominated in the deep ocean (Canfield et al., 2008; Hood and Wallace, 2015; Li et al., 2012).

5.5. Evolution of Neoproterozoic-early Cambrian ocean redox conditions (~750–510 Ma)

Secular variation in the oxygenation state of the Cryogenian ocean can be reconstructed based on seawater Mo isotope compositions. Dahl et al. (2011) reported $\delta^{98}Mo_{SW}$ of +1.11‰ for the ~750-Ma Walcott Member of the Chuar Group, Grand Canyon, which formed in a rift

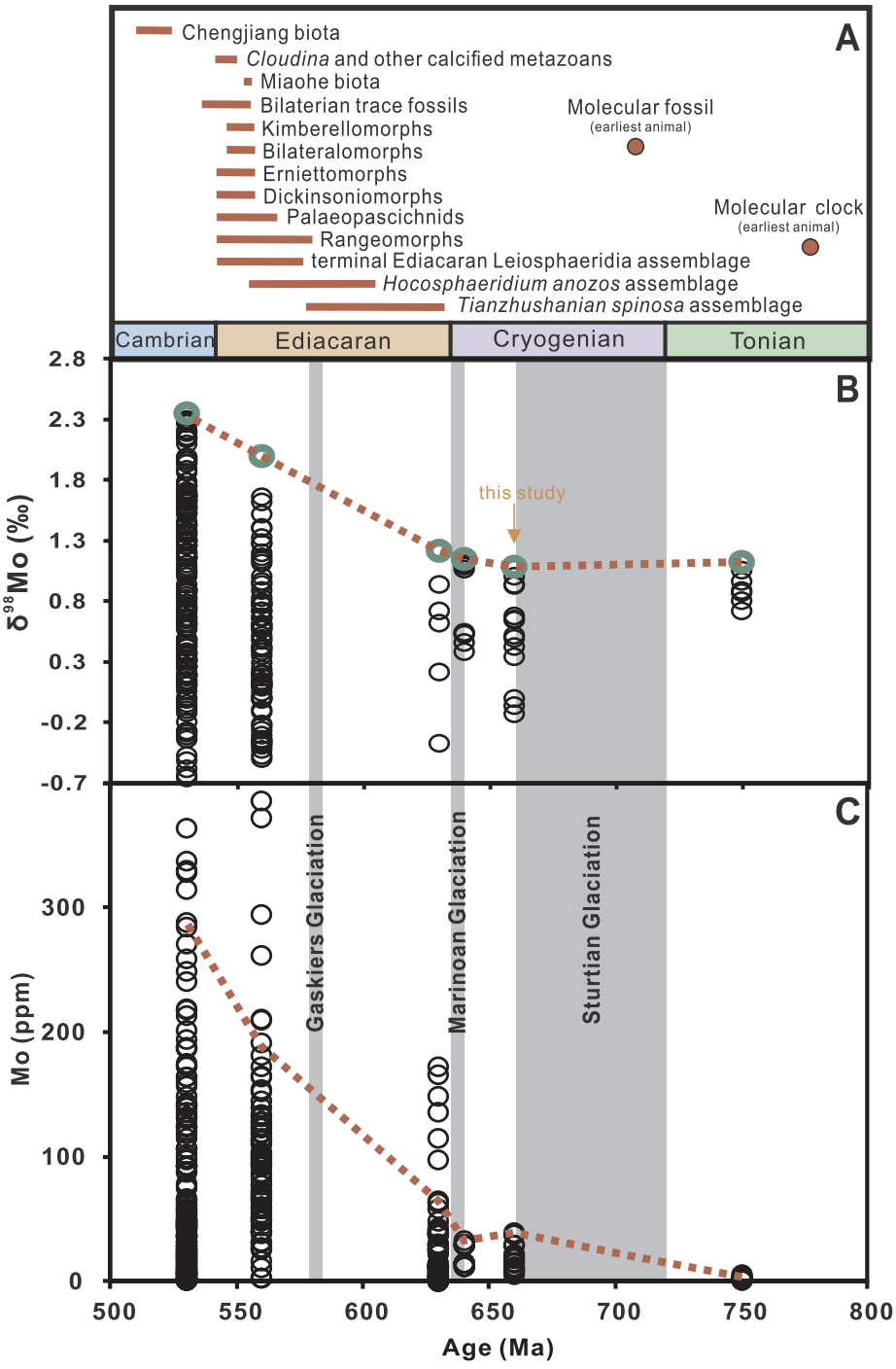

Fig. 6. Biological evolution (A), sedimentary Mo isotopes (B) and Mo concentrations (C) during 750–510 Ma. Mo isotope and concentration data are from Neoproterozoic euxinic marine facies. Biological data sources: Erwin et al. (2011), Love et al. (2009), Peterson et al. (2004), Xiao et al. (2016); δ^{98}Mo data sources: Chen et al. (2015, 2016), Cheng et al. (2017), Dahl et al. (2011), Kendall et al. (2015), Kurzweil et al. (2015), Wen et al. (2015) and this study; Mo concentration data sources: Chen et al. (2015, 2016), Dahl et al. (2011), Feng et al. (2010), Kendall et al. (2015), Kurzweil et al. (2015), Sahoo et al. (2012), Li et al. (2012), Wen et al. (2015), Cheng et al. (2017). To give a first order constraint on the evolution, we merged the sample ages to several key points: 750 Ma, 660 Ma, 640 Ma, 630 Ma, 560 Ma and 530 Ma.

basin with a connection to the open ocean. Kendall et al. (2015) reported $\delta^{98}Mo_{SW}$ of +1.15‰ for the ~640-Ma upper Black River Dolomite in Tasmania. These $\delta^{98}Mo_{SW}$ values are almost exactly the same as our results for the ~660-Ma Datangpo black shales (Fig. 6B). In addition, all three formations show similar low Mo concentrations (Fig. 6C). These observations suggest that the average oxygenation state of the global ocean did not change significantly from 750 Ma to 640 Ma, which is consistent with the argument proposed by Kunzmann et al. (2015). However, this does not preclude local changes in redox conditions. Furthermore, the existing seawater Mo isotope data are relatively sparse, so there may have been fluctuations in ocean-redox conditions during the 750–640-Ma interval that are not yet recognized. For example, Baldwin et al. (2013) reported δ^{98}Mo of +0.7‰ for a syn-Sturtian-age iron formation and argued for a $\delta^{98}Mo_{sw}$ of +1.8‰. However, Mo isotopic fractionation during adsorption by Fe oxides is a process related to pH and to the diagenetic history of the Fe oxides (Goldberg et al., 2009), which is unknown for the oceans of this period. Nevertheless, such transient events are not contradictory to our main inference, i.e., that anoxic waters dominated in the Cryogenian ocean, which is consistent with the conclusions of Canfield et al. (2008) and Guilbaud et al. (2015).

Oceanic conditions during the Ediacaran were different from those of the Cryogenian. Episodic increases in oxygen levels in Ediacaran oceans have been inferred from a wide range of proxies including Fe speciation (Canfield et al., 2007), trace elements (Partin et al., 2013; Scott et al., 2008), C–S isotopes (Fike et al., 2006; Kunzmann et al., 2017; Li et al., 2017a; McFadden et al., 2008), chemiluminescence (Wang et al., 2015), Ce anomalies (Wallace et al., 2017), Zn/Fe ratios

(Liu et al., 2016), I/(Ca + Mg) ratios (Hardisty et al., 2017), and many other indicators. The earliest oxygenation event might occur in the wake of the Marinoan Glaciation at ~630 Ma (Sahoo et al., 2012). Although Mo isotope data are lacking, the Mo concentrations of euxinic facies show a pronounced increase at that time (Fig. 6C). From ~630 Ma to 550 Ma, δ^{98}Mo in the Doushantuo Formation increased to +2.0‰, which is close to the modern seawater value of +2.3‰ (Fig. 6B) (Kendall et al., 2015). At the same time, the seawater Mo reservoir may have increased to a size similar to that of the modern ocean (Scott et al., 2008). Thus, both Mo concentration and Mo isotope data indicate that the oxygen levels of the atmosphere-ocean system were higher in the Ediacaran than in the Cryogenian. $\delta^{98}Mo_{SW}$ may have reached modern values for the first time in the early Cambrian at ~521 Ma (Chen et al., 2015) or slightly earlier (Wen et al., 2011), corresponding to permanent (Chen et al., 2015) or episodic (Dahl et al., 2017, 2010) or stepwise (Jin et al., 2016; Li et al., 2017b) oxygenation of the ocean, any of which may have triggered the Cambrian Explosion (Jin et al., 2016; Knoll and Carroll, 1999; Li et al., 2017b).

The evolution of seawater Mo isotopes and reservoir size from ~750 Ma to 510 Ma (Fig. 6) indicates a persistently anoxic Cryogenian ocean, with evidence of oxygen buildup beginning only at ~630 Ma. On the other hand, increases in atmospheric oxygen levels (> 0.1% PAL) likely began around 750–800 Ma (Blamey et al., 2016; Cole et al., 2016; Frei et al., 2009; Planavsky et al., 2014), which was 120–170 Myr earlier than evidence for substantial oceanic oxygenation. A modeling study by Reinhard et al. (2016b) argued that, under low atmospheric oxygen levels (< 2.5% PAL), dissolved oxygen concentrations in the ocean are largely controlled by marine productivity. This inference may be supported by evidence of a fundamental shift in the marine phosphorus cycle between ~800 and 635 Ma, as suggested by recent compilation and biogeochemical modeling of global P data (Reinhard et al., 2016a): specifically, increasing marine P availability enhanced oceanic productivity, finally leading to greater oxygenation of Ediacaran oceans. On the other hand, an elevated influx of reductants such as Fe^{2+} in the Cryogenian (as inferred by the global appearance of iron formation) (Konhauser et al., 2017; Kump and Seyfried, 2005) may have buffered oceanic oxygenation during the Cryogenian. Further research is needed to fully explain the delay in oceanic oxygenation following an atmospheric O_2 rise at 750–800 Ma.

5.6. Implications for the emergence and diversification of early animals

Oxygenation of the atmosphere-ocean system has been widely regarded as the trigger for the emergence and diversification of animals during the Neoproterozoic and Cambrian (e.g. Knoll and Carroll, 1999; Li et al., 2017b), although the relationship between these events might be quite complicated (e.g. Erwin, 2015; Erwin et al., 2011). Molecular clocks (Peterson et al., 2004), fossil steroids (Love et al., 2009) and possible sponge fossils (Maloof et al., 2010) place the earliest metazoan appearances in the Cryogenian Period (Fig. 6A). However, the earliest undisputed body fossil assemblages with macroscopic and morphologically complex life forms (Yuan et al., 2011), as well as other complex multicellular eukaryotes, such as possible embryos of early metazoans (Xiao et al., 1998) and sponges (Yin et al., 2015), are found in the Ediacaran (Fig. 6A). Due to the physiological need of animals for O_2, metazoan evolution during the Ediacaran is thought to have been facilitated by increased oxygen availability in the ocean (e.g. Fike et al., 2006; McFadden et al., 2008). However, experiments have recently shown that early sessile animals may have survived at oxygen levels of 0.5–4% PAL (Mills et al., 2014). Furthermore, Fe speciation data do not support a statistically significant increase in oceanic oxygen concentrations during the Ediacaran, indicating that animal diversification probably depended not on a large rise in oxygen levels but, rather, an increase past critical functional and ecological thresholds (Sperling et al., 2015). Therefore, existing evidence and the results of the present study indicate that this critical oceanic oxygenation first developed likely in the Ediacaran rather than in the Cryogenian, which is consistent with the early evolution of the animals. In other words, although atmospheric oxygen levels during ~800–750 Ma may have increased, the persistent oceanic anoxia of the Cryogenian may have delayed the diversification of metazoans until the Ediacaran.

6. Conclusions

In order to explore the oxygenation state of the Cryogenian ocean, we carried out Mo isotopic analyses of the ~660-Ma Datangpo black shales in the Minle section of the Nanhua Basin, South China, and compared these data to previously published ocean-redox proxies. Our study found:

(1) Iron speciation data indicate a continuously euxinic depositional environment during deposition of the studied black shale succession.
(2) The Nanhua Basin was a silled basin that had an open connection to the global ocean during deposition of the lower part of the black shale succession (0–6 m) but that developed increasing watermass restriction during deposition of the upper part of the black shale succession (6–20 m).
(3) Datangpo black shales yield Mo isotopes in two clusters. The lower black shales have uniformly high δ^{98}Mo values [+1.06 ± 0.06 (SD) ‰] that are inferred to reflect the δ^{98}Mo of contemporaneous seawater (ca. +1.1‰), and the upper black shales have more variable, lower δ^{98}Mo values (+0.65 ± 0.31‰) that reflect fractionations due to $[H_2S]_{aq}$ below the 11 M threshold.
(4) Seawater δ^{98}Mo was constant around +1.1‰ from ~750 to 640 Ma, indicating dominantly anoxic conditions in the global ocean. The oxygenation of the ocean was delayed relative to that of the atmosphere by an interval of 120–170 Myr, likely causing a delayed diversification of early metazoans until the Ediacaran.

Acknowledgments

We thank Zi-Hu Zhang, Li-Dan Lei, Na Li, Hai-Yang Wang, Wei Shi, Ting Zhang, Zhi-Fang Hu and Shi-Da Tang for laboratory assistance. This study is funded by the NKRD Program of China (grant 2016YFA0601100), the NSFC-RCUK_NERC Program (Grant 41661134048), the Fundamental Research Funds for Central Universities (CUG-Wuhan; Grant 1610491T01 and G1323531767) and GPMR program (GPMR201705). Lian-Jun Feng and Meng Cheng acknowledge funding by the NSFC (Grants 41072145 to LF, Grants 41703008 to MC).

References

Algeo, T.J., Maynard, J.B., 2004. Trace-element behavior and redox facies in core shales of Upper Pennsylvanian Kansas-type cyclothems. Chem. Geol. 206, 289–318.
Algeo, T.J., Lyons, T.W., 2006. Mo-total organic carbon covariation in modern anoxic marine environments: Implications for analysis of paleoredox and paleohydrographic conditions. Paleoceanography 21. http://dx.doi.org/10.1029/2004pa001112.
Anbar, A.D., Knoll, A.H., 2002. Proterozoic ocean chemistry and evolution: A bioinorganic bridge? Science 297, 1137–1142.
Archer, C., Vance, D., 2008. The isotopic signature of the global riverine molybdenum flux and anoxia in the ancient oceans. Nat. Geosci. 1, 597–600.
Arnold, G.L., Anbar, A.D., Barling, J., Lyons, T.W., 2004. Molybdenum isotope evidence for widespread anoxia in mid-Proterozoic oceans. Science 304, 87–90.
Arnold, G.L., Lyons, T.W., Gordon, G.W., Anbar, A.D., 2012. Extreme change in sulfide concentrations in the Black Sea during the Little Ice Age reconstructed using molybdenum isotopes. Geology 40, 595–598.
Baldwin, G.J., Nägler, T.F., Greber, N.D., Turner, E.C., Kamber, B.S., 2013. Mo isotopic composition of the mid-Neoproterozoic ocean: An iron formation perspective. Precambr. Res. 230, 168–178.
Barling, J., Arnold, G.L., Anbar, A.D., 2001. Natural mass-dependent variations in the isotopic composition of molybdenum. Earth Planet. Sci. Lett. 193, 447–457.
Barling, J., Anbar, A.D., 2004. Molybdenum isotope fractionation during adsorption by manganese oxides. Earth Planet. Sci. Lett. 217, 315–329.
Blamey, N.J.F., Brand, U., Parnell, J., Spear, N., Lécuyer, C., Benison, K., Meng, F., Ni, P., 2016. Paradigm shift in determining Neoproterozoic atmospheric oxygen. Geology

44, 651–654.
Brocks, J.J., Jarrett, A.J.M., Sirantoine, E., Hallmann, C., Hoshino, Y., Liyanage, T., 2017. The rise of algae in Cryogenian oceans and the emergence of animals. Nature 548, 578–581.
Canfield, D.E., 1999. The evolution of the sulfur cycle. Am. J. Sci. 299, 697–723.
Canfield, D.E., Poulton, S.W., Narbonne, G.M., 2007. Late-Neoproterozoic deep-ocean oxygenation and the rise of animal life. Science 315, 92–95.
Canfield, D.E., Poulton, S.W., Knoll, A.H., Narbonne, G.M., Ross, G., Goldberg, T., Strauss, H., 2008. Ferruginous conditions dominated later neoproterozoic deep-water chemistry. Science 321, 949–952.
Chen, X., Ling, H.F., Vance, D., Shields-Zhou, G.A., Zhu, M., Poulton, S.W., Och, L.M., Jiang, S.Y., Li, D., Cremonese, L., Archer, C., 2015. Rise to modern levels of ocean oxygenation coincided with the Cambrian radiation of animals. Nat. Commun. 6, 7.
Cheng, M., Li, C., Zhou, L., Algeo, T.J., Zhang, F., Romaniello, S., Jin, C.-S., Lei, L.-D., Feng, L.-J., Jiang, S.-Y., 2016. Marine Mo biogeochemistry in the context of dynamically euxinic mid-depth waters: A case study of the lower Cambrian Niutitang shales, South China. Geochim. Cosmochim. Acta 183, 79–93.
Cheng, M., Li, C., Zhou, L., Feng, L., Algeo, T.J., Zhang, F., Romaniello, S., Jin, C., Ling, H., Jiang, S., 2017. Transient deep-water oxygenation in the early Cambrian Nanhua Basin, South China. Geochim. Cosmochim. Acta 210, 42–58.
Cole, D.B., Reinhard, C.T., Wang, X., Gueguen, B., Halverson, G.P., Gibson, T., Hodgskiss, M.S., McKenzie, N.R., Lyons, T.W., Planavsky, N.J., 2016. A shale-hosted Cr isotope record of low atmospheric oxygen during the Proterozoic. Geology 44 (G37787), 37781.
Cole, D.B., Zhang, S., Planavsky, N.J., 2017. A new estimate of detrital redox-sensitive metal concentrations and variability in fluxes to marine sediments. Geochim. Cosmochim. Acta 215, 337–353.
Collier, R.W., 1985. Molybdenum in the northeast Pacific Ocean. Limnol. Oceanogr. 30, 1351–1354.
Condon, D., Zhu, M., Bowring, S., Wang, W., Yang, A., Jin, Y., 2005. U-Pb ages from the neoproterozoic Doushantuo Formation, China. Science 308, 95–98.
Dahl, T.W., Hammarlund, E.U., Anbar, A.D., Bond, D.P.G., Gill, B.C., Gordon, G.W., Knoll, A.H., Nielsen, A.T., Schovsbo, N.H., Canfield, D.E., 2010. Devonian rise in atmospheric oxygen correlated to the radiations of terrestrial plants and large predatory fish. Proc. Natl. Acad. Sci. USA 107, 17911–17915.
Dahl, T.W., Canfield, D.E., Rosing, M.T., Frei, R.E., Gordon, G.W., Knoll, A.H., Anbar, A.D., 2011. Molybdenum evidence for expansive sulfidic water masses in ~750 Ma oceans. Earth Planet. Sci. Lett. 311, 264–274.
Dahl, T.W., Chappaz, A., Fitts, J.P., Lyons, T.W., 2013a. Molybdenum reduction in a sulfidic lake: Evidence from X-ray absorption fine-structure spectroscopy and implications for the Mo paleoproxy. Geochim. Cosmochim. Acta 103, 213–231.
Dahl, T.W., Ruhl, M., Hammarlund, E.U., Canfield, D.E., Rosing, M.T., Bjerrum, C.J., 2013b. Tracing euxinia by molybdenum concentrations in sediments using handheld X-ray fluorescence spectroscopy (HHXRF). Chem. Geol. 360–361, 241–251.
Dahl, T.W., Chappaz, A., Hoek, J., McKenzie, C.J., Svane, S., Canfield, D.E., 2016. Evidence of molybdenum association with particulate organic matter under sulfidic conditions. Geobiology 15, 311–323.
Dahl, T.W., Connelly, J.N., Kouchinsky, A., Gill, B.C., Månsson, S.F., Bizzarro, M., 2017. Reorganisation of Earth's biogeochemical cycles briefly oxygenated the oceans 520 Myr ago. Geochem. Perspect. Lett. 3, 210–220.
Erwin, D.H., Laflamme, M., Tweedt, S.M., Sperling, E.A., Pisani, D., Peterson, K.J., 2011. The Cambrian conundrum: early divergence and later ecological success in the early history of animals. Science 334, 1091–1097.
Erwin, D.H., 2015. Early metazoan life: divergence, environment and ecology. Philos. Trans. R. Soc. B 370.
Feng, L.-J., Chu, X.-L., Huang, J., Zhang, Q.-R., Chang, H.-J., 2010. Reconstruction of paleo-redox conditions and early sulfur cycling during deposition of the Cryogenian Datangpo Formation in South China. Gondwana Res. 18, 632–637.
Fike, D.A., Grotzinger, J.P., Pratt, L.M., Summons, R.E., 2006. Oxidation of the Ediacaran ocean. Nature 444, 744–747.
Frei, R., Gaucher, C., Poulton, S.W., Canfield, D.E., 2009. Fluctuations in Precambrian atmospheric oxygenation recorded by chromium isotopes. Nature 461, 250–253.
Gilleaudeau, G.J., Frei, R., Kaufman, A.J., Kah, L.C., Azmy, K., Bartley, J.K., Chernyavskiy, P., Knoll, A.H., 2016. Oxygenation of the mid-Proterozoic atmosphere: clues from chromium isotopes in carbonates. Geochem. Perspect. Lett. 2, 178–187.
Goldberg, T., Archer, C., Vance, D., Poulton, S.W., 2009. Mo isotope fractionation during adsorption to Fe (oxyhydr)oxides. Geochim. Cosmochim. Acta 73, 6502–6516.
Goldberg, T., Gordon, G., Izon, G., Archer, C., Pearce, C.R., McManus, J., Anbar, A.D., Rehkämper, M., 2013. Resolution of inter-laboratory discrepancies in Mo isotope data: an intercalibration. J. Annal. Atom. Spectrom. 28, 724–735.
Guilbaud, R., Poulton, S.W., Butterfield, N.J., Zhu, M., Shields-Zhou, G.A., 2015. A global transition to ferruginous conditions in the early Neoproterozoic oceans. Nat. Geosci. 8, 466–470.
Hardisty, D.S., Lu, Z., Bekker, A., Diamond, C.W., Gill, B.C., Jiang, G., Kah, L.C., Knoll, A.H., Loyd, S.J., Osburn, M.R., Planavsky, N.J., Wang, C., Zhou, X., Lyons, T.W., 2017. Perspectives on Proterozoic surface ocean redox from iodine contents in ancient and recent carbonate. Earth Planet. Sci. Lett. 463, 159–170.
Helz, G.R., Miller, C.V., Charnock, J.M., Mosselmans, J.F.W., Pattrick, R.A.D., Garner, C.D., Vaughan, D.J., 1996. Mechanism of molybdenum removal from the sea and its concentration in black shales: EXAFS evidence. Geochim. Cosmochim. Acta 60, 3631–3642.
Helz, G.R., Bura-Nakić, E., Mikac, N., Ciglenečki, I., 2011. New model for molybdenum behavior in euxinic waters. Chem. Geol. 284, 323–332.
Hoffman, P.F., Kaufman, A.J., Halverson, G.P., Schrag, D.P., 1998. A Neoproterozoic Snowball Earth. Science 281, 1342–1346.
Hood, A.V.S., Wallace, M.W., 2015. Extreme ocean anoxia during the Late Cryogenian recorded in reefal carbonates of Southern Australia. Precambr. Res. 261, 96–111.
Hoshino, Y., Poshibaeva, A., Meredith, W., Snape, C., Poshibaev, V., Versteegh, G.J.M., Kuznetsov, N., Leider, A., van Maldegem, L., Neumann, M., Naeher, S., Moczydlowska, M., Brocks, J.J., Jarrett, A.J.M., Tang, Q., Xiao, S., McKirdy, D., Das, S.K., Alvaro, J.J., Sansjofre, P., Hallmann, C., 2017. Cryogenian evolution of stigmasteroid biosynthesis. Sci. Adv. 3, e1700887.
Jiang, G., Kennedy, M.J., Christie-Blick, N., 2003. Stable isotopic evidence for methane seeps in Neoproterozoic postglacial cap carbonates. Nature 426, 822–826.
Jiang, G., Shi, X., Zhang, S., Wang, Y., Xiao, S., 2011. Stratigraphy and paleogeography of the Ediacaran Doushantuo Formation (ca. 635–551 Ma) in South China. Gondwana Res. 19, 831–849.
Jin, C., Li, C., Algeo, T.J., Planavsky, N.J., Cui, H., Yang, X., Zhao, Y., Zhang, X., Xie, S., 2016. A highly redox-heterogeneous ocean in South China during the early Cambrian (~529–514 Ma): Implications for biota-environment co-evolution. Earth Planet. Sci. Lett. 441, 38–51.
Kendall, B., Creaser, R.A., Gordon, G.W., Anbar, A.D., 2009. Re–Os and Mo isotope systematics of black shales from the Middle Proterozoic Velkerri and Wollogorang Formations, McArthur Basin, northern Australia. Geochim. Cosmochim. Acta 73, 2534–2558.
Kendall, B., Komiya, T., Lyons, T.W., Bates, S.M., Gordon, G.W., Romaniello, S.J., Jiang, G.Q., Creaser, R.A., Xiao, S.H., McFadden, K., Sawaki, Y., Tahata, M., Shu, D.G., Han, J., Li, Y., Chu, X.L., Anbar, A.D., 2015. Uranium and molybdenum isotope evidence for an episode of widespread ocean oxygenation during the late Ediacaran Period. Geochim. Cosmochim. Acta 156, 173–193.
Kendall, B., Dahl, T.W., Anbar, A.D., 2017. The stable isotope geochemistry of molybdenum. Rev. Mineral. Geochem. 82, 683–732.
Knoll, A.H., Carroll, S.B., 1999. Early animal evolution: Emerging views from comparative biology and geology. Science 284, 2129–2137.
Konhauser, K.O., Planavsky, N.J., Hardisty, D.S., Robbins, L.J., Warchola, T.J., Haugaard, R., Lalonde, S.V., Partin, C.A., Oonk, P.B.H., Tsikos, H., Lyons, T.W., Bekker, A., Johnson, C.M., 2017. Iron formations: A global record of Neoarchaean to Palaeoproterozoic environmental history. Earth-Sci. Rev.
Kump, L.R., Seyfried, W.E., 2005. Hydrothermal Fe fluxes during the Precambrian: Effect of low oceanic sulfate concentrations and low hydrostatic pressure on the composition of black smokers. Earth Planet. Sci. Lett. 235, 654–662.
Kunzmann, M., Halverson, G.P., Scott, C., Minarik, W.G., Wing, B.A., 2015. Geochemistry of Neoproterozoic black shales from Svalbard: Implications for oceanic redox conditions spanning Cryogenian glaciations. Chem. Geol. 417, 383–393.
Kunzmann, M., Bui, T.H., Crockford, P.W., Halverson, G.P., Scott, C., Lyons, T.W., Wing, B.A., 2017. Bacterial sulfur disproportionation constrains timing of Neoproterozoic oxygenation. Geology 45, 207–210.
Kurzweil, F., Drost, K., Pašava, J., Wille, M., Taubald, H., Schoeckle, D., Schoenberg, R., 2015. Coupled sulfur, iron and molybdenum isotope data from black shales of the Teplá-Barrandian unit argue against deep ocean oxygenation during the Ediacaran. Geochim. Cosmochim. Acta 171, 121–142.
Lau, K.V., Macdonald, F.A., Maher, K., Payne, J.L., 2017. Uranium isotope evidence for temporary ocean oxygenation in the aftermath of the Sturtian Snowball Earth. Earth Planet. Sci. Lett. 458, 282–292.
Li, C., Love, G.D., Lyons, T.W., Fike, D.A., Sessions, A.L., Chu, X., 2010. A stratified redox model for the Ediacaran ocean. Science 328, 80–83.
Li, C., Love, G.D., Lyons, T.W., Scott, C.T., Feng, L., Huang, J., Chang, H., Zhang, Q., Chu, X., 2012. Evidence for a redox stratified Cryogenian marine basin, Datangpo Formation, South China. Earth Planet. Sci. Lett. 331–332, 246–256.
Li, C., Planavsky, N.J., Shi, W., Zhang, Z., Zhou, C., Cheng, M., Tarhan, L.G., Luo, G., Xie, S., 2015. Ediacaran marine redox heterogeneity and early animal ecosystems. Sci. Rep. 5, 8.
Li, C., Hardisty, D.S., Luo, G., Huang, J., Algeo, T.J., Cheng, M., Shi, W., An, Z., Tong, J., Xie, S., Jiao, N., Lyons, T.W., 2017a. Uncovering the spatial heterogeneity of Ediacaran carbon cycling. Geobiology 15, 211–224.
Li, C., Jin, C., Planavsky, N.J., Algeo, T.J., Cheng, M., Yang, X., Zhao, Y., Xie, S., 2017b. Coupled oceanic oxygenation and metazoan diversification during the early–middle Cambrian? Geology 45, 743–746.
Li, Z.X., Li, X.H., Kinny, P.D., Wang, J., Zhang, S., Zhou, H., 2003. Geochronology of Neoproterozoic syn-rift magmatism in the Yangtze Craton, South China and correlations with other continents: evidence for a mantle superplume that broke up Rodinia. Precambr. Res. 122, 85–109.
Li, Z.X., Bogdanova, S.V., Collins, A.S., Davidson, A., De Waele, B., Ernst, R.E., Fitzsimons, I.C.W., Fuck, R.A., Gladkochub, D.P., Jacobs, J., Karlstrom, K.E., Lu, S., Natapov, L.M., Pease, V., Pisarevsky, S.A., Thrane, K., Vernikovsky, V., 2008. Assembly, configuration, and break-up history of Rodinia: A synthesis. Precambr. Res. 160, 179–210.
Liu, X.M., Kah, L.C., Knoll, A.H., Cui, H., Kaufman, A.J., Shahar, A., Hazen, R.M., 2016. Tracing Earth's O_2 evolution using Zn/Fe ratios in marine carbonates. Geochem. Perspect. Lett. 2, 24–34.
Love, G.D., Grosjean, E., Stalvies, C., Fike, D.A., Grotzinger, J.P., Bradley, A.S., Kelly, A.E., Bhatia, M., Meredith, W., Snape, C.E., Bowring, S.A., Condon, D.J., Summons, R.E., 2009. Fossil steroids record the appearance of Demospongiae during the Cryogenian period. Nature 457, 718–721.
Lyons, T.W., Severmann, S., 2006. A critical look at iron paleoredox proxies: New insights from modern euxinic marine basins. Geochim. Cosmochim. Acta 70, 5698–5722.
Maloof, A.C., Rose, C.V., Beach, R., Samuels, B.M., Calmet, C.C., Erwin, D.H., Poirier, G.R., Yao, N., Simons, F.J., 2010. Possible animal-body fossils in pre-Marinoan limestones from South Australia. Nat. Geosci. 3, 653–659.
McFadden, K.A., Huang, J., Chu, X., Jiang, G., Kaufman, A.J., Zhou, C., Yuan, X., Xiao, S., 2008. Pulsed oxidation and biological evolution in the Ediacaran Doushantuo Formation. Proc. Natl. Acad. Sci. USA 105, 3197–3202.

McLennan, S.M., 2001. Relationships between the trace element composition of sedimentary rocks and upper continental crust. Geochem. Geophys. Geosyst. 2. http://dx.doi.org/10.1029/2000GC000109.
McManus, J., Nägler, T.F., Siebert, C., Wheat, C.G., Hammond, D.E., 2002. Oceanic molybdenum isotope fractionation: Diagenesis and hydrothermal ridge-flank alteration. Geochem. Geophys. Geosyst. 3, 1–9.
Miller, C.A., Peucker-Ehrenbrink, B., Walker, B.D., Marcantonio, F., 2011. Re-assessing the surface cycling of molybdenum and rhenium. Geochim. Cosmochim. Acta 75, 7146–7179.
Mills, D.B., Ward, L.M., Jones, C., Sweeten, B., Sweeten, M., Forth, M., Alexander, H.T., Canfield, D.E., 2014. Oxgen requirements of the earliest animals. Proc. Natl. Acad. Sci. USA 111, 4168–4172.
Morford, J.L., Martin, W.R., François, R., Carney, C.M., 2009. A model for uranium, rhenium, and molybdenum diagenesis in marine sediments based on results from coastal locations. Geochim. Cosmochim. Acta 73, 2938–2960.
Nägler, T.F., Neubert, N., Böttcher, M.E., Dellwig, O., Schnetger, B., 2011. Molybdenum isotope fractionation in pelagic euxinia: Evidence from the modern Black and Baltic Seas. Chem. Geol. 289, 1–11.
Neubert, N., Nägler, T.F., Böttcher, M.E., 2008. Sulfidity controls molybdenum isotope fractionation into euxinic sediments: Evidence from the modern Black Sea. Geology 36, 775–778.
Och, L.M., Shields-Zhou, G.A., 2012. The Neoproterozoic oxygenation event: Environmental perturbations and biogeochemical cycling. Earth-Sci Rev 110, 26–57.
Partin, C.A., Bekker, A., Planavsky, N.J., Scott, C.T., Gill, B.C., Li, C., Podkovyrov, V., Maslov, A., Konhauser, K.O., Lalonde, S.V., Love, G.D., Poulton, S.W., Lyons, T.W., 2013. Large-scale fluctuations in Precambrian atmospheric and oceanic oxygen levels from the record of U in shales. Earth Planet. Sci. Lett. 369–370, 284–293.
Peterson, K.J., Lyons, J.B., Nowak, K.S., Takacs, C.M., Wargo, M.J., McPeek, M.A., 2004. Estimating metazoan divergence times with a molecular clock. Proc. Natl. Acad. Sci. USA 101, 6536–6541.
Planavsky, N.J., Reinhard, C.T., Wang, X., Thomson, D., McGoldrick, P., Rainbird, R.H., Johnson, T., Fischer, W.W., Lyons, T.W., 2014. Low mid-Proterozoic atmospheric oxygen levels and the delayed rise of animals. Science 346, 635–638.
Poulson, B.R.L., McManus, J., Severmann, S., Berelson, W.M., 2009. Molybdenum behavior during early diagenesis: Insights from Mo isotopes. Geochem. Geophys. Geosyst. 10, 258–266.
Poulson, R.L., Siebert, C., McManus, J., Berelson, W.M., 2006. Authigenic molybdenum isotope signatures in marine sediments. Geology 34, 617–620.
Poulton, S.W., Canfield, D.E., 2011. Ferruginous conditions: A dominant feature of the ocean through Earth's history. Elements 7, 107–112.
Raiswell, R., Canfield, D.E., 1998. Sources of iron for pyrite formation in marine sediments. Am. J. Sci. 298, 219–245.
Reinhard, C.T., Planavsky, N.J., Robbins, L.J., Partin, C.A., Gill, B.C., Lalonde, S.V., Bekker, A., Konhauser, K.O., Lyons, T.W., 2013. Proterozoic ocean redox and biogeochemical stasis. Proc. Natl. Acad. Sci. USA 110, 5357–5362.
Reinhard, C.T., Planavsky, N.J., Gill, B.C., Ozaki, K., Robbins, L.J., Lyons, T.W., Fischer, W.W., Wang, C., Cole, D.B., Konhauser, K.O., 2016a. Evolution of the global phosphorus cycle. Nature 541.
Reinhard, C.T., Planavsky, N.J., Olson, S.L., Lyons, T.W., Erwin, D.H., 2016b. Earth's oxygen cycle and the evolution of animal life. Proc. Natl. Acad. Sci. USA 113.
Reitz, A., Wille, M., Nagler, T., Delange, G., 2007. Atypical Mo isotope signatures in eastern Mediterranean sediments. Chem. Geol. 245, 1–8.
Sahoo, S.K., Planavsky, N.J., Kendall, B., Wang, X., Shi, X., Scott, C., Anbar, A.D., Lyons, T.W., Jiang, G., 2012. Ocean oxygenation in the wake of the Marinoan glaciation. Nature 489, 546–549.
Scott, C., Lyons, T.W., Bekker, A., Shen, Y., Poulton, S.W., Chu, X., Anbar, A.D., 2008. Tracing the stepwise oxygenation of the Proterozoic ocean. Nature 452, 456–459.
Scott, C., Lyons, T.W., 2012. Contrasting molybdenum cycling and isotopic properties in euxinic versus non-euxinic sediments and sedimentary rocks: Refining the paleoproxies. Chem. Geol. 324, 19–27.
Siebert, C., Nägler, T.F., von Blanckenburg, F., Kramers, J.D., 2003. Molybdenum isotope records as a potential new proxy for paleoceanography. Earth Planet. Sci. Lett. 211, 159–171.
Siebert, C., McManus, J., Bice, A., Poulson, R., Berelson, W.M., 2006. Molybdenum isotope signatures in continental margin marine sediments. Earth Planet. Sci. Lett. 241, 723–733.
Sperling, E.A., Wolock, C.J., Morgan, A.S., Gill, B.C., Kunzmann, M., Halverson, G.P., Macdonald, F.A., Knoll, A.H., Johnston, D.T., 2015. Statistical analysis of iron geochemical data suggests limited late Proterozoic oxygenation. Nature 523, 451–454.
Swanson-Hysell, N.L., Rose, C.V., Calmet, C.C., Halverson, G.P., Hurtgen, M.T., Maloof, A.C., 2010. Cryogenian glaciation and the onset of carbon-isotope decoupling. Science 328, 608–611.
Tessin, A., Sheldon, N.D., Hendy, I., Chappaz, A., 2016. Iron limitation in the Western Interior Seaway during the Late Cretaceous OAE 3 and its role in phosphorus recycling and enhanced organic matter preservation. Earth Planet. Sci. Lett. 449, 135–144.
Voegelin, A.R., Pettke, T., Greber, N.D., von Niederhäusern, B., Nägler, T.F., 2014. Magma differentiation fractionates Mo isotope ratios: Evidence from the Kos Plateau Tuff (Aegean Arc). Lithos 190–191, 440–448.
Wallace, M.W., Hood, A.V., Shuster, A., Greig, A., Planavsky, N.J., Reed, C.P., 2017. Oxygenation history of the Neoproterozoic to early Phanerozoic and the rise of land plants. Earth Planet. Sci. Lett. 466, 12–19.
Wang, H., Li, C., Hu, C., Xie, S., 2015. Spurious thermoluminescence characteristics of the Ediacaran Doushantuo Formation (ca. 635–551 Ma) and its implications for marine dissolved organic carbon reservoir. J. Earth Sci. 26, 883–892.
Wang, J., Li, Z.X., 2003. History of Neoproterozoic rift basins in South China: implications for Rodinia break-up. Precambr. Res. 122, 141–158.
Wen, H., Carignan, J., Zhang, Y., Fan, H., Cloquet, C., Liu, S., 2011. Molybdenum isotopic records across the Precambrian-Cambrian boundary. Geology 39, 775–778.
Wen, H., Fan, H., Zhang, Y., Cloquet, C., Carignan, J., 2015. Reconstruction of early Cambrian ocean chemistry from Mo isotopes. Geochim. Cosmochim. Acta 164, 1–16.
Wille, M., Nägler, T.F., Lehmann, B., Schröder, S., Kramers, J.D., 2008. Hydrogen sulphide release to surface waters at the Precambrian/Cambrian boundary. Nature 453, 767–769.
Xiao, S., Zhang, Y., Knoll, A.H., 1998. Three-dimensional preservation of algae and animal embryos in a Neoproterozoic phosphorite. Nature 391, 553–558.
Xiao, S., Laflamme, M., 2009. On the eve of animal radiation: phylogeny, ecology and evolution of the Ediacara biota. Trends Ecol. Evol. 24, 31–40.
Xiao, S., Narbonne, G.M., Zhou, C., Laflamme, M., Grazhdankin, D.V., Moczydlowska-Vidal, M., Cui, H., 2016. Towards an ediacaran time scale: problems, protocols, and prospects. Episodes 39, 540.
Yang, J., Barling, J., Siebert, C., Fietzke, J., Stephens, E., Halliday, A.N., 2017. The molybdenum isotopic compositions of I-, S- and A-type granitic suites. Geochim. Cosmochim. Acta 205, 168–186.
Yin, Z., Zhu, M., Davidson, E.H., Bottjer, D.J., Zhao, F., Tafforeau, P., 2015. Sponge grade body fossil with cellular resolution dating 60 Myr before the Cambrian. Proc. Natl. Acad. Sci. USA 112, E1453–1460.
Yuan, X., Chen, Z., Xiao, S., Zhou, C., Hua, H., 2011. An early Ediacaran assemblage of macroscopic and morphologically differentiated eukaryotes. Nature 470, 390–393.
Zerkle, A.L., House, C.H., Cox, R.P., Canfield, D.E., 2006. Metal limitation of cyanobacterial N_2 fixation and implications for the Precambrian nitrogen cycle. Geobiology 4, 285–297.
Zhang, F., Yan, B., Guo, Y., Zhu, X., Zhou, Q., Yang, D., 2013. Precipitation form of manganese ore deposites in Gucheng, Hubei Province, and its paleoenvironment implication. Acta Geol. Sin. 87, 245–258.
Zhang, F., Zhu, X., Yan, B., Kendall, B., Peng, X., Li, J., Algeo, T.J., Romaniello, S., 2015. Oxygenation of a Cryogenian ocean (Nanhua Basin, South China) revealed by pyrite Fe isotope compositions. Earth Planet. Sci. Lett. 429, 11–19.
Zhang, S., Jiang, G., Han, Y., 2008. The age of the Nantuo Formation and Nantuo glaciation in South China. Terra Nova 20, 289–294.
Zhou, C., Tucker, R., Xiao, S., Peng, Z., Yuan, X., Chen, Z., 2004. New constraints on the ages of Neoproterozoic glaciations in south China. Geology 32, 437.